

Extreme conditions in a dissolving air nanobubble

Kyuichi Yasui,* Toru Tuziuti, and Wataru Kanematsu

*National Institute of Advanced Industrial Science and Technology (AIST)
2266-98 Anagahora, Shimoshidami, Moriyama-ku, Nagoya 463-8560, Japan*

(Received 17 February 2016; revised manuscript received 2 June 2016; published 11 July 2016)

Numerical simulations of the dissolution of an air nanobubble in water have been performed taking into account the effect of bubble dynamics (inertia of the surrounding liquid). The presence of stable bulk nanobubbles is not assumed in the present study because the bubble radius inevitably passes the nanoscale in the complete dissolution of a bubble. The bubble surface is assumed to be clean because attachment of hydrophobic materials on the bubble surface could considerably change the gas diffusion rate. The speed of the bubble collapse (the bubble wall speed) increases to about 90 m/s or less. The shape of a bubble is kept nearly spherical because the amplitude of the nonspherical component of the bubble shape is negligible compared to the instantaneous bubble radius. In other words, a bubble never disintegrates into daughter bubbles during the dissolution. At the final moment of the dissolution, the temperature inside a bubble increases to about 3000 K due to the quasiadiabatic compression. The bubble temperature is higher than 1000 K only for the final 19 ps. However, the Knudsen number is more than 0.2 for this moment, and the error associated with the continuum model should be considerable. In the final 2.3 ns, only nitrogen molecules are present inside a bubble as the solubility of nitrogen is the lowest among the gas species. The radical formation inside a bubble is negligible because the probability of nitrogen dissociation is only on the order of 10^{-15} . The pressure inside a bubble, as well as the liquid pressure at the bubble wall, increases to about 5 GPa at the final moment of dissolution. The pressure is higher than 1 GPa for the final 0.7 ns inside a bubble and for the final 0.6 ns in the liquid at the bubble wall. The liquid temperature at the bubble wall increases to about 360 K from 293 K at the final stage of the complete dissolution.

DOI: [10.1103/PhysRevE.94.013106](https://doi.org/10.1103/PhysRevE.94.013106)**I. INTRODUCTION**

Air bubbles in water are very frequently formed in the sea, lakes, rivers, and any kinds of water on the earth [1,2]. They are formed by liquid surface waves as well as by rain drops and waterfalls. After the formation, many bubbles disappear at the liquid surface by buoyancy. Many other bubbles completely dissolve into the water before reaching the liquid surface [3]. The situation is the same for air bubbles in water in a liquid container in a laboratory. When the bubble size is smaller, the probability of complete dissolution into water is higher as the time for complete dissolution is shorter [4,5]. Such tiny air bubbles could be created by acoustic or hydrodynamic cavitation [5–7]. Machines such as microbubble and nanobubble generators are commercially available [8]. Tiny bubbles less than 1 μm in diameter are called nanobubbles or ultrafine bubbles [9–13]. Many nanobubbles completely dissolve in water because the time for complete dissolution is usually shorter than the time for reaching the liquid surface by buoyancy.

The time for complete dissolution of a gas bubble into liquid has been calculated by the Epstein-Plesset theory [4,5]. According to the theory, it is 77.8 μs for an air bubble in water saturated with air when the initial bubble radius is 100 nm. In the theory, however, the effect of bubble dynamics (the effect of the inertia of the surrounding liquid) is completely neglected. Although there are several theoretical and experimental studies on the dissolution of a bubble, the effect has been completely neglected [14–26].

It has been suggested by some researchers that OH radicals are created at the final moment of the dissolution of a gas bubble into water [3,13]. In acoustic and hydrodynamic cavitation, on the other hand, a bubble initially expands due to the decrease in liquid pressure by ultrasound or by some hydrodynamic motion. Then a bubble violently collapses, which is called the Rayleigh collapse [5,27]. The violent collapse is due to the inertia of the surrounding liquid as well as the geometry of a spherical collapse. In this case, the temperature and pressure inside a bubble increase to several thousand Kelvin and several hundred atmospheres or more, respectively [27–29]. The extreme conditions inside a bubble are confirmed by the spectra of sonoluminescence which is the light emission associated with the violent bubble collapse [27,30]. Due to the extreme conditions, OH radicals are created through the dissociation of water vapor inside cavitation bubbles [31–36]. There have been many numerical studies on the Rayleigh collapse and the creation of OH radicals inside a collapsing bubble [29,33,37–41]. The direct comparison between the experimental and numerical results is possible for a single-bubble system in which a single bubble is trapped near the pressure antinode of a standing ultrasonic field in partially degassed water [32,33]. The theoretical model by the authors for numerical simulations has been validated from the studies of single-bubble sonoluminescence and sonochemistry which is chemistry associated with the violent bubble collapse under ultrasound [33,42]. For the Rayleigh collapse, the expansion of a bubble by the decrease in liquid pressure by ultrasound or by some hydrodynamic motion is required [5]. In the simple dissolution of an air bubble into water, it has been widely believed that the bubble collapse is not violent as assumed in the Epstein-Plesset theory [4,5]. In the present paper, we have performed numerical simulations

*k.yasui@aist.go.jp

of the simple dissolution of an air bubble into water taking into account the effect of bubble dynamics (the inertia of the surrounding liquid). When a bubble completely dissolves into water, the bubble radius inevitably passes the nanometer scale. Thus, the presence of stable nanobubbles, which is still under debate [9–12,43–45], is not assumed in the present study.

II. MODEL

The model of bubble dynamics used in the present numerical simulations has been described in Refs. [29,33,46–48]. It has been validated from studies of single-bubble sonoluminescence and sonochemistry [33,42]. There is only one important modification in the model in the present study, that the effect of the gas (air) diffusion from the interior of a bubble into the surrounding water is taken into account by Eq. (1). Here, the bubble surface is assumed to be clean because the attachment of hydrophobic materials to the bubble surface could considerably change the gas diffusion rate [45].

$$\frac{dn_i}{dt} = -4\pi R^2 D_i \frac{(c_{s,i} - c_{\infty,i})}{R}, \quad (1)$$

where n_i is the number of molecules inside a bubble for the gas species i ($i = \text{N}_2, \text{O}_2$, or Ar), t is time, R is the instantaneous bubble radius, D_i is the diffusion coefficient of the gas species i in the liquid, $c_{s,i}$ is the saturated concentration of the species i in the liquid at the bubble wall, and $c_{\infty,i}$ is the concentration of the gas species i in the liquid far from a bubble. In the Epstein-Plesset theory, Eq. (1) is analytically solved without taking into account the effect of the inertia of the surrounding liquid [4,5]. In Eq. (1), it is assumed that the gas concentration profile is in a steady state and that the liquid medium is quiescent. A non-steady-state concentration profile results in the higher rate of gas diffusion. On the other hand, movement of the liquid medium results in the lower rate of gas diffusion due to the shell effect [7]. Thus, the two effects may roughly compensate. Although the compensation may not be perfect, Eq. (1) is a standard equation of the gas diffusion from the interior of a bubble because it has been used in the Epstein-Plesset theory. Thus, Eq. (1) is used in the present study although further studies are required on the deviation from Eq. (1).

The diffusion coefficients in liquid water are calculated as a function of the liquid temperature at the bubble wall by using the following equation.

$$D_i = B_i e^{-\frac{\Delta E_i}{R_g T_{L,i}}}, \quad (2)$$

where B_i and ΔE_i are the preexponential constant and the activation energy, respectively, for the gas species i ; R_g is the gas constant ($=8.31 \text{ J/mol K}$); and $T_{L,i}$ is the liquid temperature at the bubble wall. B_i and ΔE_i for each gas species are listed in Table I [49].

The saturated gas concentration ($c_{s,i}$) of the species i in the liquid is calculated by the Henry's law constant. The equations for the Henry's law constants as a function of temperature are given in Appendix A. The saturated gas concentration at the bubble wall is calculated by Eq. (3).

$$c_{s,i} = \frac{10^3 \rho_{L,i} N_A p_g}{K_{H,i} M_{\text{H}_2\text{O}}} \left(\frac{n_i}{n_t} \right), \quad (3)$$

TABLE I. B_i and ΔE_i in Eq. (2) for the diffusion coefficient of each gas species in liquid water [49].

	B_i (m ² /s)	ΔE_i (J/mol)
N ₂	7.9×10^{-6}	1.963×10^4
O ₂	4.2×10^{-6}	1.838×10^4
Ar	10.6×10^{-6}	2.064×10^4

where $\rho_{L,i}$ is the instantaneous liquid density at the bubble wall [47], N_A is the Avogadro number [$=6.02 \times 10^{23}$ (/mol)], p_g is the instantaneous pressure inside a bubble, $K_{H,i}$ is the Henry's law constant of the gas species i at the instantaneous liquid temperature ($T_{L,i}$) at the bubble wall, $M_{\text{H}_2\text{O}}$ is the molecular weight of H₂O ($=18 \text{ g/mol}$), n_i is the instantaneous number of molecules of the gas species i inside a bubble, and n_t is the instantaneous total number of molecules inside a bubble. The gas concentration ($c_{\infty,i}$) far from a bubble in the liquid is calculated by Eq. (4).

$$c_{\infty,i} = \frac{10^3 \rho_{L,\infty} N_A p_0}{K_{H,i,\infty} M_{\text{H}_2\text{O}}} r_i, \quad (4)$$

where $\rho_{L,\infty}$ is the ambient liquid density, p_0 is the ambient static pressure ($=1 \text{ atm} = 1.013 \times 10^5 \text{ Pa}$), $K_{H,i,\infty}$ is the Henry's law constant of the gas species i at the ambient liquid temperature (T_∞), and r_i is the molar ratio of the gas species i in air ($r_{\text{N}_2} = 0.78$, $r_{\text{O}_2} = 0.21$, $r_{\text{Ar}} = 0.01$). The values of the gas concentration ($c_{\infty,i}$) far from a bubble are as follows: 0.55 mol/m^3 for N₂, 0.29 mol/m^3 for O₂, and 0.015 mol/m^3 for Ar. The solubility is the lowest for N₂ as the solubility of each gas species at each gas pressure of 1 atm at 20 °C is as follows: 0.71 mol/m^3 for N₂, 1.39 mol/m^3 for O₂, and 1.53 mol/m^3 for Ar.

In the present numerical simulations, it is assumed that a bubble completely disappears when the total number of molecules inside a bubble is smaller than 1. In the model of bubble dynamics, the following effects are taken into account: nonequilibrium evaporation and condensation of water vapor at the bubble wall, thermal conduction both inside and outside a bubble, and temporal variation of the liquid temperature at the bubble wall. The physical properties in liquid water at the bubble wall are calculated as a function of temperature and pressure at the bubble wall such as the liquid density, sound velocity, saturated vapor pressure, thermal conductivity of the liquid, latent heat of evaporation, viscosity, surface tension, Henry's law constants, diffusion coefficients of gases, and heat of solution of gases. The equations are given in Refs. [47,50] except Henry's law constants, diffusion coefficients of gases, and heat of solution of gases given in this paper. The equations for the heat of solution of gases are given in Appendix B. The dependence of the saturated vapor pressure (p_v^*) on the bubble radius is also taken into account using Eq. (5) although the effect is negligible because at the final stage of the bubble dissolution there is no water vapor inside a bubble as seen later [51].

$$p_v^* = p_{v0}^* e^{-\frac{2\sigma V_{mL}}{R R_g T_{L,i}}}, \quad (5)$$

where p_{v0}^* is the saturated vapor pressure at a flat liquid surface as a function of temperature [47], σ is the surface tension, V_{mL}

is the molar volume of liquid water ($=1.8 \times 10^{-5} \text{ m}^3$), and R is the instantaneous bubble radius.

The sound velocity (c) in the liquid at the bubble wall is calculated by the following equation [50,52].

$$c = \sqrt{\frac{7.15(\rho_B + B)}{\rho_{L,i}}}, \quad (6)$$

where ρ_B is the liquid pressure at the bubble wall, B is the constant used in the modified Tait equation of state for the liquid water ($B = 3.049 \times 10^8 \text{ Pa}$), and $\rho_{L,i}$ is the liquid density at the bubble wall.

The dependence of the surface tension (σ) on the bubble radius is taken into account by the Tolman equation [Eq. (7)] with the Tolman length of $\delta = -0.05 \text{ nm}$ [53–56].

$$\frac{\sigma}{\sigma_0} = \frac{1}{\left(1 + \frac{2\delta}{R}\right)}, \quad (7)$$

where σ_0 is the surface tension at a flat liquid surface which is a function of the liquid temperature at the bubble wall [47].

Bubble dynamics is described by the modified Keller equation (modified Rayleigh-Plesset equation) in which the effects of the compressibility of the liquid and evaporation or condensation of water vapor at the bubble wall are taken into account [47].

$$\begin{aligned} & \left(1 - \frac{\dot{R}}{c} + \frac{\dot{m}}{c\rho_{L,i}}\right) R \ddot{R} + \frac{3}{2} \dot{R}^2 \left(1 - \frac{\dot{R}}{3c} + \frac{2\dot{m}}{3c\rho_{L,i}}\right) \\ &= \frac{1}{\rho_{L,\infty}} \left(1 + \frac{\dot{R}}{c}\right) [p_B - p_0] + \frac{\dot{m}R}{\rho_{L,i}} \left(1 - \frac{\dot{R}}{c} + \frac{\dot{m}}{c\rho_{L,i}}\right) \\ &+ \frac{\dot{m}}{\rho_{L,i}} \left(\dot{R} + \frac{\dot{m}}{2\rho_{L,i}} + \frac{\dot{m}\dot{R}}{2c\rho_{L,i}} - \frac{R}{\rho_{L,i}} \frac{d\rho_{L,i}}{dt} - \frac{\dot{m}R}{c\rho_{L,i}^2} \frac{d\rho_{L,i}}{dt}\right) \\ &+ \frac{R}{c\rho_{L,\infty}} \frac{dp_B}{dt}, \end{aligned} \quad (8)$$

where $\dot{R} = \frac{dR}{dt}$, c is the sound velocity in the liquid at the bubble wall [Eq. (6)] [50,52], \dot{m} is the rate of evaporation of water vapor at the bubble wall (negative value means condensation), $\ddot{R} = \frac{d^2R}{dt^2}$, $\rho_{L,\infty}$ is the liquid density far from a bubble ($=9.982 \times 10^2 \text{ kg/m}^3$), p_0 is the ambient static pressure, and $\dot{m} = \frac{dm}{dt}$. The equation to calculate the rate of nonequilibrium evaporation (\dot{m}) is given in Ref. [29]. p_B is estimated by Eq. (9).

$$p_B = p_g - \frac{2\sigma}{R} - \frac{4\mu\dot{R}}{R}, \quad (9)$$

where p_g is the gas pressure inside a bubble, σ is surface tension [Eq. (7)], and μ is the viscosity of the liquid as a function of liquid pressure and temperature at the bubble wall [47]. p_g is calculated by the van der Waals equation of state inside a bubble.

$$\left(p_g + \frac{a}{v^2}\right)(v - b) = R_g T, \quad (10)$$

TABLE II. The van der Waals constants of each gas species [57].

	a_i (J m ³ /mol ²)	b_i (m ³ /mol)
N ₂	1.370×10^{-1}	3.87×10^{-5}
O ₂	1.382×10^{-1}	3.186×10^{-5}
Ar	1.355×10^{-1}	3.201×10^{-5}
H ₂ O	5.537×10^{-1}	3.049×10^{-5}

where v is the molar volume, a and b are van der Waals constants, R_g is the gas constant, and T is the temperature inside a bubble. The molar volume is calculated as follows.

$$v = \frac{N_A V}{n_t}, \quad (11)$$

where V is the bubble volume, and n_t is the total number of molecules inside a bubble. The van der Waals constants are calculated by the following equations.

$$a = \frac{1}{n_t} (n_{\text{N}_2} a_{\text{N}_2} + n_{\text{O}_2} a_{\text{O}_2} + n_{\text{Ar}} a_{\text{Ar}} + n_{\text{H}_2\text{O}} a_{\text{H}_2\text{O}}), \quad (12)$$

$$b = \frac{1}{n_t} (n_{\text{N}_2} b_{\text{N}_2} + n_{\text{O}_2} b_{\text{O}_2} + n_{\text{Ar}} b_{\text{Ar}} + n_{\text{H}_2\text{O}} b_{\text{H}_2\text{O}}), \quad (13)$$

where n_{N_2} , n_{O_2} , n_{Ar} , $n_{\text{H}_2\text{O}}$ are the number of molecules of N₂, O₂, argon, and H₂O, respectively, inside a bubble, and a_{N_2} , a_{O_2} , a_{Ar} , $a_{\text{H}_2\text{O}}$ are the van der Waals constants of N₂, O₂, argon, and H₂O, respectively. The van der Waals constants for each gas species are listed in Table II [57].

Temperature is assumed to be spatially uniform inside a bubble except in the thermal boundary layer near the bubble wall. This assumption has been validated under many conditions of the Rayleigh collapse by direct numerical simulations of the fundamental equations of fluid dynamics [58]. In the present study, the temperature inside a bubble is calculated by solving the following equation [46].

$$\begin{aligned} E &= \frac{n_{\text{N}_2}}{N_A} \int_0^T C_{V,\text{N}_2}(\dot{T}) d\dot{T} + \frac{n_{\text{O}_2}}{N_A} \int_0^T C_{V,\text{O}_2}(\dot{T}) d\dot{T} \\ &+ \frac{n_{\text{Ar}}}{N_A} \int_0^T C_{V,\text{Ar}}(\dot{T}) d\dot{T} + \frac{n_{\text{H}_2\text{O}}}{N_A} \int_0^T C_{V,\text{H}_2\text{O}}(\dot{T}) d\dot{T} \\ &- \left(\frac{n_t}{N_A}\right)^2 \frac{a}{V}, \end{aligned} \quad (14)$$

where E is the thermal energy of a bubble, N_A is the Avogadro number, and $C_{V,\text{N}_2}(\dot{T})$, $C_{V,\text{O}_2}(\dot{T})$, $C_{V,\text{Ar}}(\dot{T})$, $C_{V,\text{H}_2\text{O}}(\dot{T})$ are the molar heat capacities at constant volume of N₂, O₂, argon, and H₂O, respectively, at temperature \dot{T} . The integration of the molar heat capacity of each gas species with temperature is described in Appendix C [59]. The derivation of Eq. (14) is as follows [46]. The internal energy (E) of a bubble is a function of temperature (T) and volume (V) of a bubble for the van der Waals gas. Thus

$$dE = \left(\frac{\partial E}{\partial T}\right)_V dT + \left(\frac{\partial E}{\partial V}\right)_T dV. \quad (15)$$

From the definition of molar heat capacity at constant volume, the following relationship holds.

$$\left(\frac{\partial E}{\partial T}\right)_V = \frac{n_{\text{N}_2}}{N_A} C_{V,\text{N}_2}(T) + \frac{n_{\text{O}_2}}{N_A} C_{V,\text{O}_2}(T) + \frac{n_{\text{Ar}}}{N_A} C_{V,\text{Ar}}(T) + \frac{n_{\text{H}_2\text{O}}}{N_A} C_{V,\text{H}_2\text{O}}(T). \quad (16)$$

For the van der Waals gas, the second term in Eq. (15) is nonzero [51].

$$\left(\frac{\partial E}{\partial V}\right)_T = T \left(\frac{\partial p}{\partial T}\right)_V - p_g = \left(\frac{n_i}{N_A}\right)^2 \frac{a}{V^2}. \quad (17)$$

Inserting Eqs. (16) and (17) into Eq. (15) and integrating the first term by temperature from 0 (K) to T (K) and the second term by volume from infinity to V , one obtains Eq. (14).

The thermal energy of a bubble (E) is estimated by using Eq. (18).

$$\Delta E = -p_g \Delta V + \sum_i e_i \Delta n_i + 4\pi R^2 \frac{10^3 N_A}{M_{\text{H}_2\text{O}}} \dot{m} e_{\text{H}_2\text{O}} \Delta t + 4\pi R^2 \kappa \left. \frac{\partial T}{\partial r} \right|_{r=R} \Delta t, \quad (18)$$

where ΔE is the change of the thermal energy in a small time (a time step) Δt , ΔV is the change of the bubble volume, e_i is the energy carried by a molecule of the gas species i , Δn_i is the change in the number of molecules of the gas species i inside a bubble, the summation is for all the gas species, $M_{\text{H}_2\text{O}}$ is the molecular weight of water ($= 18$ g/mol), $e_{\text{H}_2\text{O}}$ is the energy carried by an evaporating or a condensing water molecule, κ is the thermal conductivity of the gas, and $\left. \frac{\partial T}{\partial r} \right|_{r=R}$ is the temperature gradient at the bubble wall inside a bubble ($\left. \frac{\partial T}{\partial r} \right|_{r=R} = \frac{(T_B - T)}{l_{th}}$ is assumed, where T_B is the gas and vapor temperature at the bubble wall, l_{th} is the thickness of the thermal boundary layer near the bubble wall inside a bubble. l_{th} is assumed as $n\lambda$, where $n = 7$ and λ is the instantaneous mean free path of a gas molecule inside a bubble [33,60,61]).

The energy carried by a molecule of each gas species is given as follows [48].

$$e_{\text{N}_2} = \frac{1}{N_A} \int_0^{T_B} C_{V,\text{N}_2}(\acute{T}) d\acute{T}, \quad (19)$$

$$e_{\text{O}_2} = \frac{1}{N_A} \int_0^{T_B} C_{V,\text{O}_2}(\acute{T}) d\acute{T}, \quad (20)$$

$$e_{\text{Ar}} = \frac{1}{N_A} \int_0^{T_B} C_{V,\text{Ar}}(\acute{T}) d\acute{T} = \frac{3R_g T_B}{2N_A}, \quad (21)$$

$$e_{\text{H}_2\text{O}} = \frac{1}{N_A} \int_0^{T_B} C_{V,\text{H}_2\text{O}}(\acute{T}) d\acute{T}. \quad (22)$$

The thermal conductivity (κ) is calculated by the following equation [62].

$$\kappa = 0.5 \left[\sum_i x_i \kappa_i + \left\{ \sum_i \left(\frac{x_i}{\kappa_i} \right) \right\}^{-1} \right], \quad (23)$$

where x_i is the mole fraction of the gas species i inside a bubble, and κ_i is the thermal conductivity of the gas species i at temperature T . The thermal conductivity of each gas species as a function of temperature is described in Appendix D [62].

The continuity of energy flux at the bubble wall is given by the following equation.

$$\kappa_L \left. \frac{\partial T_L}{\partial r} \right|_{r=R} = \kappa \left. \frac{\partial T}{\partial r} \right|_{r=R} + \dot{m} \frac{10^3 N_A}{M_{\text{H}_2\text{O}}} (L + e_{\text{H}_2\text{O}}) + \sum_i \left[\frac{dn_i}{dt} (e_i - \Delta H_i) \right], \quad (24)$$

where κ_L is the thermal conductivity of liquid water, $\left. \frac{\partial T_L}{\partial r} \right|_{r=R}$ is the temperature gradient in liquid water at the bubble wall, L is the latent heat of evaporation or condensation of water, the summation is for all the gas species ($i = \text{N}_2, \text{O}_2, \text{and Ar}$), $\frac{dn_i}{dt}$ is the rate of the change in the number of molecules of the species i given by Eq. (1), and ΔH_i is the heat of solution of the gas species i into water (Appendix B). Using Eq. (24), the liquid temperature ($T_{L,i}$) at the bubble wall is calculated. The equations to calculate $T_{L,i}$ and T_B are given in Refs. [29,47].

On the right side of Eq. (18), the first term is pV work done by the surrounding liquid to a bubble. The second term is the energy decrease due to the gas diffusion out of a bubble. The third term is the energy exchange due to nonequilibrium evaporation or condensation of water vapor at the bubble wall. The last term is the energy exchange due to thermal conduction between the interior of a bubble and the surrounding liquid.

In order to see the degree of gas rarefaction inside a bubble, the Knudsen number (K_n) is numerically calculated as a function of time [63].

$$K_n = \frac{\lambda}{R}, \quad (25)$$

where λ is the instantaneous mean free path of a gas molecule inside a bubble, and R is the instantaneous bubble radius. The mean free path (λ) is calculated by the following equation [51].

$$\lambda = \frac{V}{\sqrt{2} \sigma n_i}, \quad (26)$$

where σ is the cross section of a molecule in the bubble and is assumed as $\sigma = 0.4 \times 10^{-18} \text{ m}^2$.

In order to see whether the quantum effect is present inside a nanobubble, the de Broglie wavelength (λ_{dB}) of a gas molecule is also calculated as a function of time [51].

$$\lambda_{\text{dB}} = \frac{h}{m\bar{v}}, \quad (27)$$

where h is the Planck constant ($= 6.626 \times 10^{-34} \text{ J s}$), m is the mass of a gas molecule ($= 4.65 \times 10^{-26} \text{ kg}$ for a N_2 molecules), and \bar{v} is the mean speed of a gas molecule given by the following equation [51].

$$\bar{v} = \sqrt{\frac{8k_B T}{\pi m}}, \quad (28)$$

where k_B is the Boltzmann constant ($= 1.38 \times 10^{-23} \text{ J/K}$), and T is the temperature inside a bubble in Kelvin.

In order to see whether thermal equilibrium is achieved inside a bubble, the mean free time (t_{mf}), which is the average

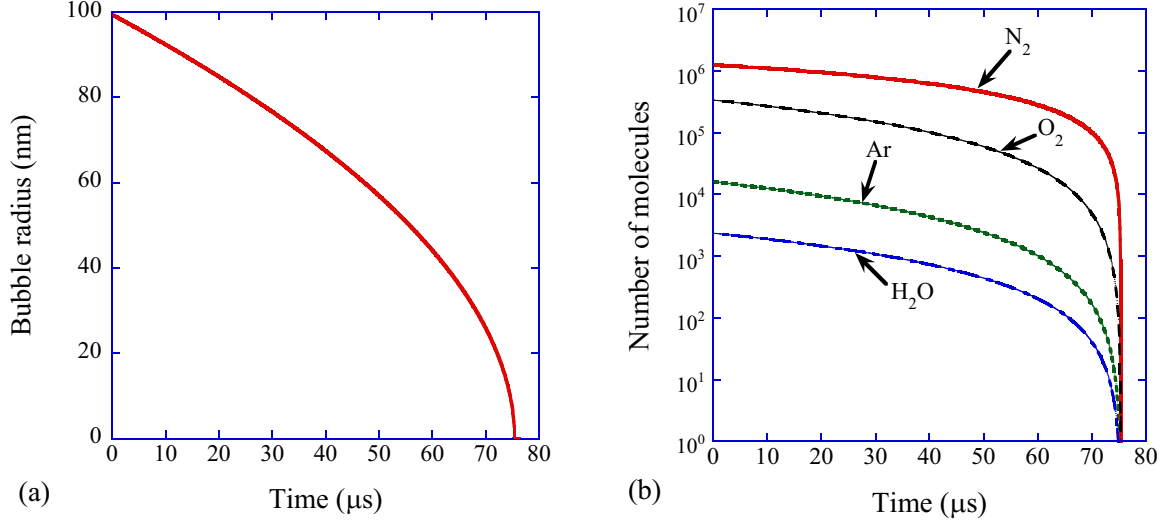


FIG. 1. The result of the numerical simulation for the dissolution of an air nanobubble into water saturated with air as a function of time for about $75.4 \mu\text{s}$. The initial bubble radius is 100 nm . (a) The bubble radius (R). (b) The number (n_i) of molecules of each gas or vapor species inside a bubble with logarithmic vertical axis.

time between collisions of a gas molecule inside a bubble, is also calculated as a function of time [51].

$$t_{mf} = \frac{\lambda}{\bar{v}}. \quad (29)$$

The density (ρ_g) inside a bubble is calculated by the following equation.

$$\rho_g = \frac{10^{-3}(n_{\text{N}_2}M_{\text{N}_2} + n_{\text{O}_2}M_{\text{O}_2} + n_{\text{Ar}}M_{\text{Ar}} + n_{\text{H}_2\text{O}}M_{\text{H}_2\text{O}})}{n_t v}, \quad (30)$$

where M_{N_2} , M_{O_2} , M_{Ar} are the molecular weight of N_2 , O_2 , and Argon, respectively ($M_{\text{N}_2} = 28$, $M_{\text{O}_2} = 32$, $M_{\text{Ar}} = 40 \text{ g/mol}$), and v is the molar volume.

In order to study the shape stability (or instability) of a bubble, the amplitude of the nonspherical component of the bubble surface is numerically calculated in the simulations [64–66]. When the amplitude of the nonspherical component exceeds the instantaneous mean bubble radius, a bubble would disintegrate into daughter bubbles. A small distortion of the spherical surface is described by $R(t) + a_n(t)Y_n$ where $R(t)$ is the instantaneous mean bubble radius at time t , Y_n is a spherical harmonic of degree n , and $a_n(t)$ is the amplitude of the nonspherical component. The dynamics for the amplitude of the nonspherical component $a_n(t)$ is given by

$$\ddot{a}_n + B_n(t)\dot{a}_n - A_n(t)a_n = 0, \quad (31)$$

where the overdot denotes the time derivative (d/dt),

$$A_n(t) = (n-1)\frac{\ddot{R}}{R} - \frac{\beta_n\sigma}{\rho R^3} - \left[(n-1)(n+2) + 2n(n+2)(n-1)\frac{\delta}{R} \right] \frac{2\mu\dot{R}}{R^3}, \quad (32)$$

and

$$B_n(t) = \frac{3\dot{R}}{R} + \left[(n+2)(2n+1) - 2n(n+2)^2\frac{\delta}{R} \right] \frac{2\mu}{R^2}, \quad (33)$$

where $\beta_n = (n-1)(n+1)(n+2)$, and δ is the thickness of the thin layer where fluid flows,

$$\delta = \min\left(\sqrt{\frac{\mu t_{\text{ch}}}{2\pi}}, \frac{R}{2n}\right), \quad (34)$$

where t_{ch} is the characteristic time.

III. RESULTS AND DISCUSSIONS

A numerical simulation is performed for the dissolution of an air nanobubble into water saturated with air. The initial bubble radius is 100 nm . According to the simulation, the time for the complete dissolution is $75.36 \mu\text{s}$ (Fig. 1). It is slightly shorter than that estimated from the Epstein-Plesset theory ($77.8 \mu\text{s}$) due to the bubble dynamics (the inertia of the surrounding liquid).

Surprisingly, the temperature inside a bubble (T) increases up to about 3000 K at the final moment of the bubble dissolution [Fig. 2(a)]. This is due to the quasiadiabatic compression of a bubble. The pV work done by the surrounding liquid slightly overwhelms the energy loss due to thermal conduction [Fig. 2(b)]. The energy loss due to the gas diffusion into the surrounding liquid does not considerably influence the bubble temperature because the temperature is determined by the thermal energy per molecule. The quasiadiabatic compression means that the bubble compression is not an ideal adiabatic process but there is considerable thermal conduction between the bubble interior and the surrounding liquid. The duration of the high temperature is very short. The temperature is higher than 1000 K for only 19 ps [Fig. 2(a)]. However, at this stage, the Knudsen number is more than 0.2 [Fig. 2(c)]. The number of molecules inside a bubble is less than 11 . Thus the error associated with the continuum model should be considerable at this final moment of the bubble dissolution. As the de Broglie wavelength is two orders of magnitude smaller than the bubble radius, the quantum effect would be negligible inside a nanobubble even near the final moment of the bubble

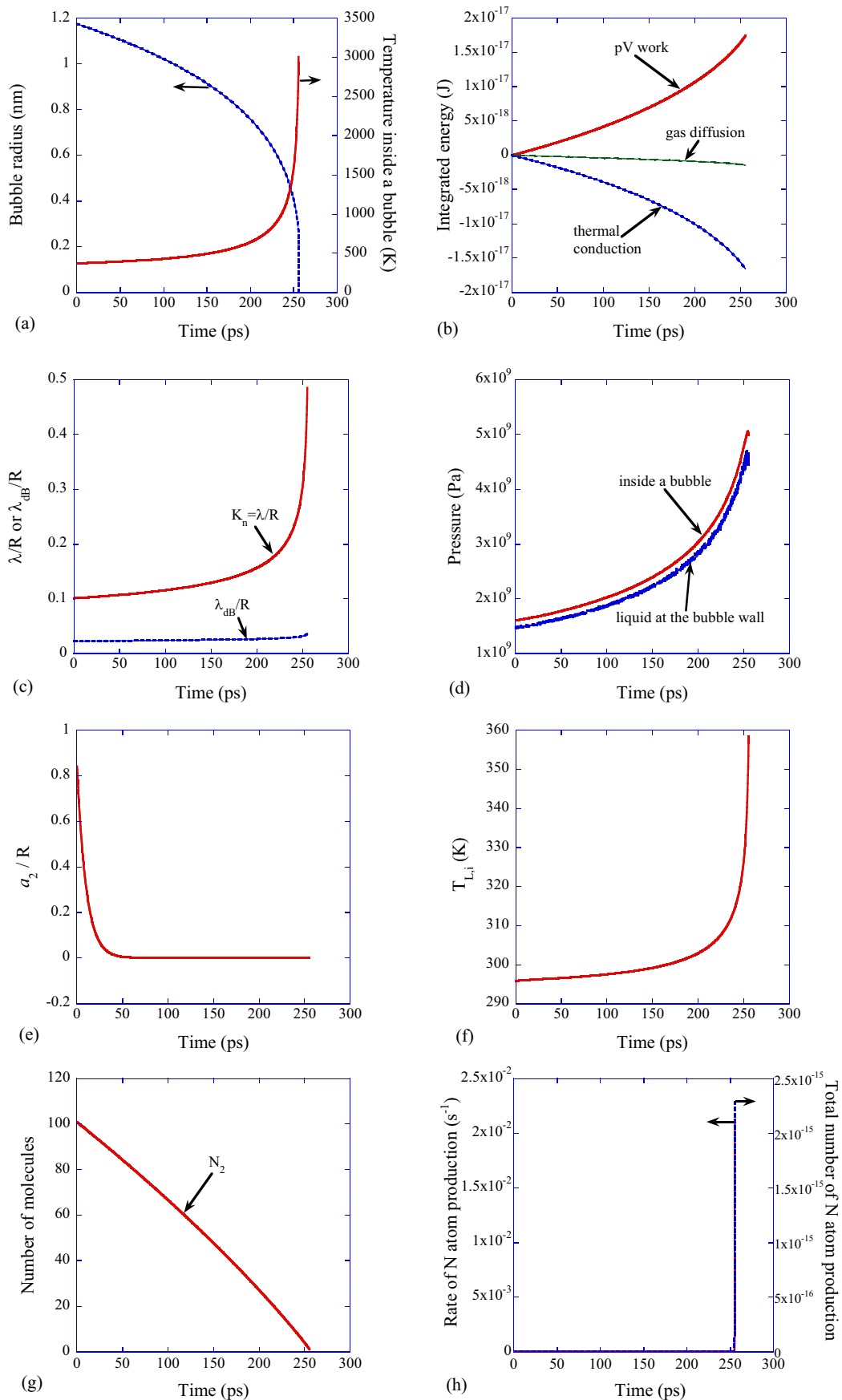


FIG. 2.

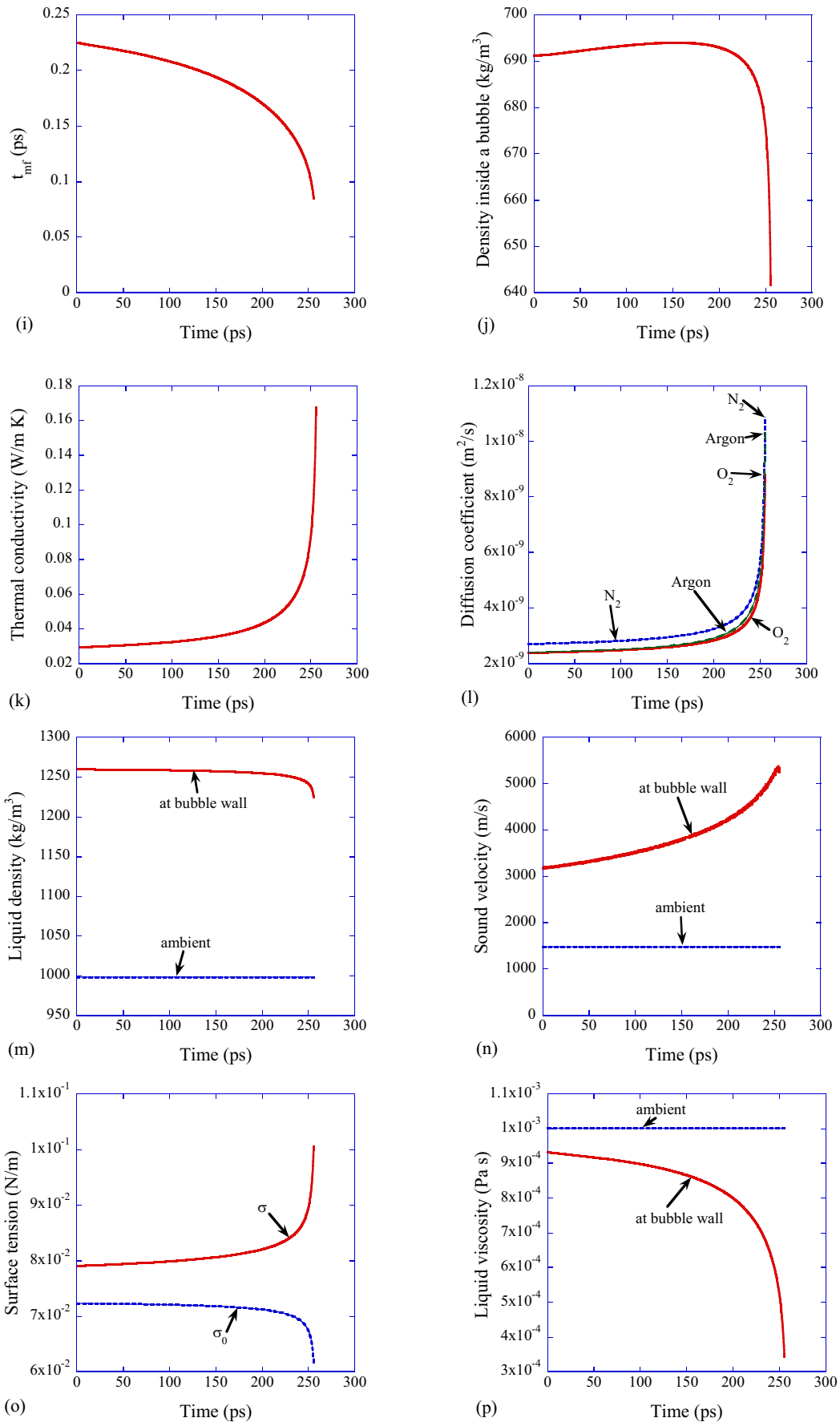


FIG. 2. (Continued.)

dissolution [Fig. 2(c)]. For much lighter gas species such as H_2 , however, some quantum effect would be possible inside a nanobubble such as discrete values of temperature and pressure because the de Broglie wavelength is much longer.

The maximum bubble wall speed reaches about $|dR/dt| = 90$ m/s. According to the present numerical simulation, the bubble wall speed temporally fluctuates during the final moment of the bubble collapse due to some computational error whereby negligibly tiny pulsation of a bubble sets in during the dissolution process. This is the reason why there is a tiny fluctuation in the liquid pressure (p_B) at the bubble wall in Fig. 2(d). However, the computational error does not influence the conclusions in the present paper. On the other hand, the computational error significantly affects the magnitude of the acoustic energy radiated from a bubble, which is not discussed in the present paper.

Surprisingly again, the liquid pressure at the bubble wall increases up to about 5 GPa at the final moment of the bubble dissolution. In a quiescent liquid model such as the Epstein-Plesset theory, the liquid pressure at the bubble wall is kept constant (1 atm) even at the final moment of the bubble dissolution. Due to the bubble dynamics (the inertia of the surrounding liquid), however, the liquid pressure significantly increases according to the present numerical simulation. As the pressure inside a bubble is higher than the liquid pressure at the bubble wall due to surface tension, the pressure inside a bubble also increases up to about 5 GPa at the final moment. The pressure is higher than 1 GPa for the final 0.7 ns inside a bubble and for the final 0.6 ns in the liquid at the bubble wall.

According to the present numerical simulations, the amplitude of the nonspherical component of a bubble is always much smaller than the instantaneous mean bubble radius [Fig. 2(e)]. Thus it is expected that the bubble shape is kept almost spherical during its dissolution. In other words, a bubble never disintegrates into daughter bubbles.

The liquid temperature ($T_{L,i}$) at the bubble wall increases up to about 358 K (85 °C) at the final moment of the bubble dissolution [Fig. 2(f)]. The liquid temperature at the bubble wall is higher than 30 °C (50 °C) for the final 53 ps (7 ps). In equilibrium, these liquid temperatures and pressures at the bubble wall at the final moment of the bubble dissolution correspond to the solid state (ice) of water [67]. Further studies are required on whether transient, high-pressure solidification of water takes place near the bubble wall. If such solidification occurs, the gas diffusion into the surrounding

water would be stopped, and a rebound of a bubble would be observed.

Initially, about 76% of the bubble content is N_2 molecules in mole fraction [Fig. 1(b)]. In the last 2.3 ns of the dissolution, the bubble content becomes only N_2 molecules as the solubility of N_2 is the lowest among the gas species, although only the last 255 ps is shown in Fig. 2(g). The increase of the liquid temperature to 85 °C is insufficient for the dissociation of liquid water. Thus the only possible radical formation is the dissociation of N_2 molecules inside a bubble (Eq. (35)).



The rate constant is given by Eq. (36) [68].

$$k = 6.1 \times 10^{-9} T^{-1.6} e^{-113200/T} \quad (\text{m}^3 \text{ molecule}^{-1} \text{ s}^{-1}), \quad (36)$$

where k is defined by $-\frac{d[N_2]}{dt} = k[N_2]^2$; $[N_2]$ is the concentration of N_2 molecules in ($\text{molecules}/\text{m}^3$), and T is temperature in K. Equation (36) may result in some error for the temperature below 6000 K because the dissociation of N_2 molecules usually takes place above 6000 K. The rate (dN_N/dt) of N atom production is given by Eq. (37).

$$\frac{dN_N}{dt} = 2k[N_2]^2 V, \quad (37)$$

where V is the bubble volume in m^3 . The total number (N_N) of N atoms produced is given by Eq. (38).

$$N_N = \int \frac{dN_N}{dt} dt. \quad (38)$$

The result of the numerical simulations is shown in Fig. 2(h). The production of N atoms is negligible because N_N is only on the order of 10^{-15} . It is due to the lower bubble temperature (3000 K) than that required for the dissociation of N_2 molecules (6000 K) as well as the small number of molecules inside a bubble and the very short duration of the high temperature inside a bubble.

However, the mean free time of gas molecules inside a bubble is about 0.1 ps at this moment [Fig. 2(i)]. It would be sufficiently small for the equilibrium of the translational motion of gas molecules because the number of collisions necessary to provide equilibrium distributions from strongly perturbed thermodynamic states of an assembly of particles is on the order of 10 for the translational motion [69,70]. It would be insufficient for the equilibrium of rotational and vibrational motion because the number of collisions necessary for them

The result of the numerical simulation as a function of time for the last 255 ps of the complete dissolution of an air nanobubble into water. The condition is the same as that in Fig. 1 ($t = 0$ in this figure corresponds to $t = 75.361 \mu\text{s}$ in Fig. 1). (a) The bubble radius (R) (dotted line) and the temperature (T) inside a bubble (solid line). (b) Temporally integrated pV work, energy loss due to thermal conduction and that by gas diffusion. (c) The Knudsen number (K_n) and the de Broglie wavelength (λ_{dB}) relative to the bubble radius (R). (d) The pressure (p_g) inside a bubble and the liquid pressure (p_B) at the bubble wall. (e) The amplitude of the nonspherical component of degree $n = 2$ relative to the instantaneous mean bubble radius. The initial a_2 is assumed as 1 nm with $da_2/dt = 0$. (f) The liquid temperature ($T_{L,i}$) at the bubble wall. (g) The number (n_{N_2}) of N_2 molecules inside a bubble. (There is no other gas and vapor species inside a bubble at the final 2.3 ns.) (h) The rate of N atom production (dN_N/dt) and the total number (N_N) of N atoms production. (i) The mean free time (t_{mf}) of gas molecules inside a bubble. (j) The density (ρ_g) inside a bubble. (k) The thermal conductivity (κ) of gas inside a bubble. (l) The diffusion coefficient (D_i) of gas in liquid water. (m) The liquid density ($\rho_{L,i}$) at the bubble wall and that ($\rho_{L,\infty}$) far from a bubble. (n) The sound velocity (c) in the liquid water at the bubble wall and that (c_0) far from a bubble. (o) The surface tension at the curved bubble surface (σ) and that at a flat surface (σ_0) as a function of the liquid temperature ($T_{L,i}$). (p) The viscosity (μ) of the liquid water at the bubble wall and that (μ_0) far from a bubble.

is on the order of 10^3 and 10^5 , respectively. Thus the error associated with Eq. (36) would be considerable.

The density inside a bubble increases up to about 690 kg/m^3 , and slightly drops at the final moment of the bubble dissolution due to the dramatic increase in temperature [Fig. 2(j)]. The density is about 86% of that of liquid nitrogen at the boiling point at 1 atm (807 kg/m^3 at 77 K). As the pressure inside a bubble is several orders of magnitude higher than the critical pressure of N_2 ($3.39 \times 10^6 \text{ Pa}$), N_2 inside a bubble is in a supercritical state (the critical temperature of N_2 is only 126 K.).

The thermal conductivity (κ) of the gas inside a bubble suddenly increases at the final moment because the temperature suddenly increases [Fig. 2(k)]. The diffusion coefficients of gas species in liquid water also suddenly increase at the final moment because the diffusion coefficients exponentially depend on the inverse of the liquid temperature ($T_{L,i}$) at the bubble wall which suddenly increases [Eq. (2)]. Although only N_2 molecules are present inside a bubble at the final moment, the diffusion coefficients of the other gases are also shown in Fig. 2(l). The liquid density ($\rho_{L,i}$) at the bubble wall is about 25% higher than that far from a bubble at the final moment because of the high pressure (p_B) of the liquid at the bubble wall [Fig. 2(m)]. The liquid density slightly drops just before the complete dissolution because of the sudden increase in the liquid temperature ($T_{L,i}$) at the bubble wall. The sound velocity (c) in the liquid water at the bubble wall increases up to about 5400 m/s as the liquid pressure at the bubble wall increases to about 5 GPa [Fig. 2(n)]. The tiny fluctuation in the sound velocity in Fig. 2(n) is due to the numerical error mentioned before. Near the final moment of the bubble dissolution, the Tolman equation results in the considerably higher surface tension (σ) than that at a flat surface (σ_0) [Fig. 2(o)]. The drop of σ_0 at the final moment is due to the increase in the liquid temperature ($T_{L,i}$) at the bubble wall. The viscosity (μ) of the liquid at the bubble wall decreases considerably as the liquid temperature ($T_{L,i}$) at the bubble wall considerably increases [Fig. 2(p)].

IV. CONCLUSION

Bubble dynamics simulation has been performed for the dissolution of an air bubble into water saturated with air. The presence of stable nanobubbles is not assumed because the radius of any bubble passes the nanoscale during the complete dissolution of the bubble. The bubble surface is assumed to be clean because the attachment of hydrophobic materials to the surface could considerably change the gas diffusion rate. For the initial radius of 100 nm, an air bubble completely dissolves into water in $75.36 \mu\text{s}$ according to the present numerical simulation. It is slightly shorter than that estimated from the Epstein-Plesset theory ($77.8 \mu\text{s}$) due to the bubble dynamics (the inertia of the surrounding liquid). The shape of a bubble is kept nearly spherical during the dissolution as the nonspherical component of the bubble shape is negligible compared to the instantaneous bubble radius. In other words, a bubble never disintegrates into daughter bubbles. Surprisingly, the temperature inside a bubble

increases to about 3000 K at the final moment of the complete dissolution due to the quasiadiabatic compression of a bubble. The bubble temperature is higher than 1000 K only for about 19 ps. However, at this moment, the Knudsen number is more than 0.2 and the error associated with the continuum model should be considerable. The pressure inside a bubble as well as the liquid pressure at the bubble wall increases to about 5 GPa. The pressure is higher than 1 GPa for the last 0.7 ns inside a bubble and for the last 0.6 ns in the liquid at the bubble wall. The liquid temperature at the bubble wall increases up to about 85°C at the final moment. As a result, physical properties of the liquid water at the bubble wall, such as density, sound velocity, surface tension, and viscosity, considerably change. The bubble content becomes only N_2 molecules at the final 2.3 ns because the solubility of N_2 is the lowest among the gas species. In spite of the extreme condition inside a bubble, the radical formation is negligible because the probability of N_2 dissociation is only on the order of 10^{-15} .

ACKNOWLEDGMENTS

The authors would like to thank Noriya Izu of AIST for useful comments. A part of this work was supported by METI, Japan, as part of the international standardization project for fine bubbles.

APPENDIX A: HENRY'S LAW CONSTANTS

The equations for the Henry's law constants ($K_{H,i}$) are assumed as follows as a function of temperature which are valid only near the room temperature.

For N_2 [71],

$$\ln \left(\frac{K_{H,\text{N}_2}}{10^9} \right) = 58.190472 - \frac{86.32129}{\tau} - 24.79808 \ln \tau, \quad (\text{A1})$$

where the Henry's law constant (K_{H,N_2}) is expressed in Pa, $\tau = \frac{T(\text{K})}{100}$, and T is the temperature in Kelvin. In the calculation of the saturated gas concentration at the bubble wall, $T = T_{L,i}$. In the calculation of the gas concentration far from a bubble, $T = T_\infty = 293.15 \text{ K}$.

For O_2 [72],

$$\ln \left(\frac{K_{H,\text{O}_2}}{10^9} \right) = 55.017904 - \frac{83.91236}{\tau} - 23.24323 \ln \tau. \quad (\text{A2})$$

For argon [73],

$$\ln \left(\frac{K_{H,\text{Ar}}}{10^9} \right) = -5.339034 + 5.448711 \times \frac{10^3}{T} - 1.026654 \times \frac{10^6}{T^2}, \quad (\text{A3})$$

where T is in Kelvin.

APPENDIX B: HEAT OF SOLUTION OF GASES

The equations for the heat of solution (ΔH_i) of gases are assumed as follows as a function of temperature which are valid only near the room temperature.

For N₂ [71],

$$\Delta H_{N_2} = \frac{1}{N_A} (-8.632\,129 \times 10^3 R_g + 2.479\,808 \times 10 R_g T_{L,i}) \left(\frac{\text{J}}{\text{molecule}} \right), \quad (\text{B1})$$

where N_A is the Avogadro number [=6.02 × 10²³ (/mol)], R_g is the gas constant (=8.31 J/mol K), and $T_{L,i}$ is the liquid temperature at the bubble wall in Kelvin.

For O₂ [72],

$$\Delta H_{O_2} = \frac{1}{N_A} (-8.391\,236 \times 10^3 R_g + 2.324\,323 \times 10 R_g T_{L,i}) \left(\frac{\text{J}}{\text{molecule}} \right). \quad (\text{B2})$$

For argon [73],

$$\Delta H_{Ar} = \frac{1}{N_A} \left(5.448\,711 \times 10^3 R_g - 2.053\,308 \times \frac{10^6 R_g}{T_{L,i}} \right) \left(\frac{\text{J}}{\text{molecule}} \right). \quad (\text{B3})$$

APPENDIX C: MOLAR ENERGY

From the formulas of specific heat for each gas species in Ref. [59], the molar energy, which is the integration of molar heat capacity at constant volume with temperature, is approximately given by the following equations.

For N₂,

For temperatures between 250 and 775 K,

$$\int_0^T C_{V,N_2}(\dot{T}) d\dot{T} = [44.412\,25 + 0.174\,037\,95(T - 250) + 1.814\,444 \times 10^{-5}(T - 250)^2] \times 4.186 \times 28 \left(\frac{\text{J}}{\text{mol}} \right). \quad (\text{C1})$$

For temperatures between 775 and 1500 K,

$$\int_0^T C_{V,N_2}(\dot{T}) d\dot{T} = [140.783\,235 + 0.197\,647\,828(T - 775) + 2.1369 \times 10^{-5}(T - 775)^2] \times 4.186 \times 28 \left(\frac{\text{J}}{\text{mol}} \right). \quad (\text{C2})$$

For temperatures above 1500 K,

$$\int_0^T C_{V,N_2}(\dot{T}) d\dot{T} = [295.31 + 0.226\,288(T - 1500)] \times 4.186 \times 28 \left(\frac{\text{J}}{\text{mol}} \right). \quad (\text{C3})$$

For O₂,

For temperatures between 250 and 775 K,

$$\int_0^T C_{V,O_2}(\dot{T}) d\dot{T} = [38.886 + 0.153\,255\,36(T - 250) + 3.4379 \times 10^{-5}(T - 250)^2] \times 4.186 \times 32 \left(\frac{\text{J}}{\text{mol}} \right). \quad (\text{C4})$$

For temperatures between 775 and 1500 K,

$$\int_0^T C_{V,O_2}(\dot{T}) d\dot{T} = [128.820\,83 + 0.190\,835\,536(T - 775) + 1.508\,933 \times 10^{-5}(T - 775)^2] \times 4.186 \times 32 \left(\frac{\text{J}}{\text{mol}} \right). \quad (\text{C5})$$

For temperatures above 1500 K,

$$\int_0^T C_{V,O_2}(\dot{T}) d\dot{T} = [275.107\,924 + 0.211\,023\,4(T - 1500)] \times 4.186 \times 32 \left(\frac{\text{J}}{\text{mol}} \right). \quad (\text{C6})$$

For H₂O (vapor),

For temperatures between 250 and 775 K,

$$\int_0^T C_{V,H_2O}(\dot{T}) d\dot{T} = [83.358\,98 + 0.325\,982\,09(T - 250) + 6.616\,16 \times 10^{-5}(T - 250)^2] \times 4.186 \times 18 \left(\frac{\text{J}}{\text{mol}} \right). \quad (\text{C7})$$

For temperatures between 775 and 1500 K,

$$\int_0^T C_{V,H_2O}(\dot{T}) d\dot{T} = [272.735\,36 + 0.400\,238\,9(T - 775) + 7.953\,117 \times 10^{-5}(T - 775)^2] \times 4.186 \times 18 \left(\frac{\text{J}}{\text{mol}} \right). \quad (\text{C8})$$

For temperatures above 1500 K,

$$\int_0^T C_{V,H_2O}(\dot{T}) d\dot{T} = [604.712\,13 + 0.512\,462\,7(T - 1500)] \times 4.186 \times 18 \left(\frac{\text{J}}{\text{mol}} \right). \quad (\text{C9})$$

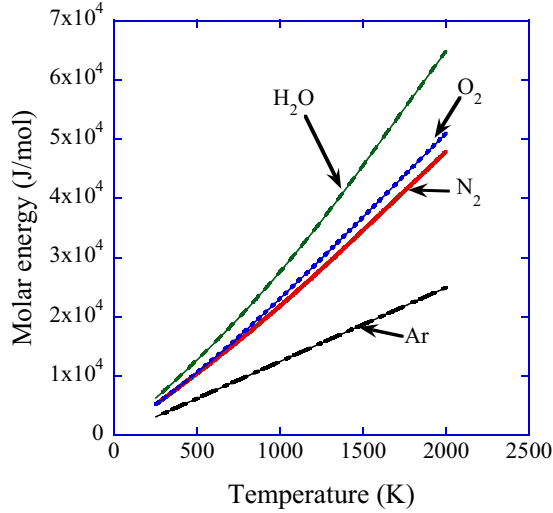


FIG. 3. The molar energy assumed in the present simulation for each gas species as a function of temperature.

For argon, the molar heat capacity is assumed to be independent of temperature as $3R_g/2$ where R_g is the gas constant ($=8.31 \text{ J/mol K}$) [59]. Thus its integration is simply given by the following equation.

$$\int_0^T C_{V,\text{Ar}} dT = \frac{3R_g T}{2} \left(\frac{\text{J}}{\text{mol}} \right). \quad (\text{C10})$$

Numerically calculated integration of the molar heat capacity is shown in Fig. 3 as a function of temperature.

APPENDIX D: THERMAL CONDUCTIVITY OF GASES AND VAPOR

From the experimental data in Ref. [62], the thermal conductivity of each gas species and vapor is estimated by the following equations as a function of temperature T in Kelvin.

For N_2 ,

$$\kappa_{\text{N}_2} = 5.22573 \times 10^{-5} T + 1.008538 \times 10^{-2} \left(\frac{\text{W}}{\text{m K}} \right). \quad (\text{D1})$$

For O_2 ,

$$\kappa_{\text{O}_2} = 6.447887 \times 10^{-5} T + 7.2211268 \times 10^{-3} \left(\frac{\text{W}}{\text{m K}} \right). \quad (\text{D2})$$

For argon,

$$\kappa_{\text{Ar}} = 3.5887 \times 10^{-5} T + 6.81277 \times 10^{-3} \left(\frac{\text{W}}{\text{m K}} \right). \quad (\text{D3})$$

For H_2O (vapor),

$$\kappa_{\text{H}_2\text{O}} = 9.967213 \times 10^{-5} T - 1.1705 \times 10^{-2} \left(\frac{\text{W}}{\text{m K}} \right). \quad (\text{D4})$$

- [1] *Natural Physical Sources of Underwater Sound: Sea Surface Sound*, edited by B. R. Kerman (Kluwer Academic, Dordrecht, 1993).
- [2] R. Clift, J. R. Grace, and M. E. Weber, *Bubbles, Drops, and Particles* (Dover, New York, 2005).
- [3] M. Takahashi, K. Chiba, and P. Li, Free-radical generation from collapsing microbubbles in the absence of a dynamic stimulus, *J. Phys. Chem. B* **111**, 1343 (2007).
- [4] P. S. Epstein and M. S. Plesset, On the stability of gas bubbles in liquid-gas solutions, *J. Chem. Phys.* **18**, 1505 (1950).
- [5] K. Yasui, Dynamics of acoustic bubbles, in *Sonochemistry and the Acoustic Bubble*, edited by F. Grieser, P. K. Choi, N. Enomoto, H. Harada, K. Okitsu, and K. Yasui (Elsevier, Amsterdam, 2015), Chap. 3, pp. 41–83.
- [6] F. R. Young, *Cavitation* (Imperial College Press, London, 1999).
- [7] T. G. Leighton, *The Acoustic Bubble* (Academic Press, London, 1994).
- [8] *Micro- and Nanobubbles*, edited by H. Tsuge (Pan Stanford, Singapore, 2014).
- [9] T. Tuziuti, K. Yasui, and W. Kanematsu, Measurement of the change in the number of ultrafine bubbles through pressurization, Proc. SPIE **9232**, 92320T (2014), edited by N. Aya, N. Iki, T. Shimura, and T. Shirai (OPC2014 in Tokyo).
- [10] H. Kobayashi, S. Maeda, M. Kashiwa, and T. Fujita, Measurement and identification of ultrafine bubbles by resonant mass measurement method, Proc. SPIE **9232**, 92320S (2014), edited by N. Aya, N. Iki, T. Shimura, and T. Shirai (OPC2014 in Tokyo).
- [11] H. Kobayashi, S. Maeda, M. Kashiwa, and T. Fujita, Measurements of ultrafine bubbles using different types of particle size measuring instruments, Proc. SPIE **9232**, 92320U (2014), edited by N. Aya, N. Iki, T. Shimura, and T. Shirai (OPC2014 in Tokyo).
- [12] S. Maeda, H. Kobayashi, K. Ida, M. Kashiwa, I. Nishihara, and T. Fujita, The effect of dilution on the quantitative measurement of bubbles in high-density ultrafine bubble-filled water using the light scattering method, Proc. SPIE **9232**, 92320V (2014), edited by N. Aya, N. Iki, T. Shimura, and T. Shirai (OPC2014 in Tokyo).
- [13] S. Liu, S. Oshita, Y. Makino, Q. Wang, Y. Kawagoe, and T. Uchida, Oxidative capacity of nanobubbles and its effect on seed germination, *ACS Sustainable Chem. Eng.* **4**, 1347 (2016).
- [14] J. M. Solano-Altamirano, J. D. Malcolm, and S. Goldman, Gas bubble dynamics in soft materials, *Soft Matter* **11**, 202 (2015).
- [15] G. Kapodistrias and P. H. Dahl, Scattering measurements from a dissolving bubble, *J. Acoust. Soc. Am.* **131**, 4243 (2012).
- [16] J. J. Kwan and M. A. Borden, Microbubble dissolution in a multigas environment, *Langmuir* **26**, 6542 (2010).
- [17] K. Sarkar, A. Katiyar, and P. Jain, Growth and dissolution of an encapsulated contrast microbubble: Effects of encapsulation permeability, *Ultrasound Med. Biol.* **35**, 1385 (2009).

- [18] M. M. Lozano, E. Talu, and M. L. Longo, Dissolution of microbubbles generated in seawater obtained offshore: Behavior and surface tension measurements, *J. Geophys. Res.* **112**, C12001 (2007).
- [19] S. Kentish, J. Lee, M. Davidson, and M. Ashokkumar, The dissolution of a stationary spherical bubble beneath a flat plate, *Chem. Eng. Sci.* **61**, 7697 (2006).
- [20] P. B. Duncan and D. Needham, Test of the Epstein-Plesset model for gas microparticle dissolution in aqueous media: Effect of surface tension and gas undersaturation in solution, *Langmuir* **20**, 2567 (2004).
- [21] M. A. Borden and M. L. Longo, Dissolution behavior of lipid monolayer-coated, air-filled microbubbles: Effect of lipid hydrophobic chain length, *Langmuir* **18**, 9225 (2002).
- [22] S. Ljunggren and J. C. Eriksson, The lifetime of a colloid-sized gas bubble in water and the cause of the hydrophobic attraction, *Colloids Surf., A* **129–130**, 151 (1997).
- [23] J. L. Duda and J. S. Vrentas, Heat or mass transfer-controlled dissolution of a isolated sphere, *Int. J. Heat Mass Transfer* **14**, 395 (1971).
- [24] J. L. Duda and J. S. Vrentas, Mathematical analysis of bubble dissolution, *AIChE J.* **15**, 351 (1969).
- [25] M. Cable and D. J. Evans, Spherically symmetrical diffusion-controlled growth or dissolution of a sphere, *J. Appl. Phys.* **38**, 2899 (1967).
- [26] I. M. Krieger, G. W. Mulholland, and C. S. Dickey, Diffusion coefficients for gases in liquids from the rates of solution of small gas bubbles, *J. Phys. Chem.* **71**, 1123 (1967).
- [27] M. P. Brenner, S. Hilgenfeldt, and D. Lohse, Single-bubble sonoluminescence, *Rev. Mod. Phys.* **74**, 425 (2002).
- [28] K. S. Suslick, N. C. Eddingsaas, D. J. Flannigan, S. D. Hopkins, and H. Xu, Extreme conditions during multibubble cavitation: Sonoluminescence as a spectroscopic probe, *Ultrason. Sonochem.* **18**, 842 (2011).
- [29] K. Yasui, Alternative model of single-bubble sonoluminescence, *Phys. Rev. E* **56**, 6750 (1997).
- [30] F. R. Young, *Sonoluminescence* (CRC Press, Boca Raton, FL, 2005).
- [31] K. Makino, M. M. Mossoba, and P. Riesz, Chemical effects of ultrasound on aqueous solutions. Evidence for OH and H by spin trapping, *J. Am. Chem. Soc.* **104**, 3537 (1982).
- [32] Y. T. Didenko and K. S. Suslick, The energy efficiency of formation of photons, radicals and ions during single-bubble cavitation, *Nature (London)* **418**, 394 (2002).
- [33] K. Yasui, T. Tuziuti, M. Sivakumar, and Y. Iida, Theoretical study of single-bubble sonochemistry, *J. Chem. Phys.* **122**, 224706 (2005).
- [34] A. Henglein, Contributions to various aspects of cavitation chemistry, *Adv. Sonochem.* **3**, 17 (1993), edited by T. J. Mason (JAI Press, London).
- [35] C. von Sonntag, G. Mark, A. Tauber, and H. P. Schuchmann, OH radical formation and dosimetry in the sonolysis of aqueous solutions, *Adv. Sonochem.* **5**, 109 (1999).
- [36] *Theoretical and Experimental Sonochemistry Involving Inorganic Systems*, edited by Pankaj and M. Ashokkumar (Springer, Dordrecht, 2011).
- [37] B. D. Storey and A. J. Szeri, Water vapour, sonoluminescence and sonochemistry, *Proc. R. Soc. London, Ser. A* **456**, 1685 (2000).
- [38] K. Yasui, T. Tuziuti, Y. Iida, and H. Mitome, Theoretical study of the ambient-pressure dependence of sonochemical reactions, *J. Chem. Phys.* **119**, 346 (2003).
- [39] K. Yasui, T. Tuziuti, T. Kozuka, A. Towata, and Y. Iida, Relationship between the bubble temperature and main oxidant created inside an air bubble under ultrasound, *J. Chem. Phys.* **127**, 154502 (2007).
- [40] K. Yasui, T. Tuziuti, J. Lee, T. Kozuka, A. Towata, and Y. Iida, The range of ambient radius for an active bubble in sonoluminescence and sonochemical reactions, *J. Chem. Phys.* **128**, 184705 (2008).
- [41] K. Yasui and K. Kato, Bubble dynamics and sonoluminescence from helium or xenon in mercury and water, *Phys. Rev. E* **86**, 036320 (2012).
- [42] K. Yasui, Single-bubble sonoluminescence from noble gases, *Phys. Rev. E* **63**, 035301(R) (2001).
- [43] D. Lohse and X. Zhang, Surface nanobubbles and nanodroplets, *Rev. Mod. Phys.* **87**, 981 (2015).
- [44] A. Habich, W. Ducker, D. E. Dunstan, and X. Zhang, Do stable nanobubbles exist in mixtures of organic solvents and water?, *J. Phys. Chem. B* **114**, 6962 (2010).
- [45] K. Yasui, T. Tuziuti, W. Kanematsu, and K. Kato, Dynamic equilibrium model for a bulk nanobubble and a microbubble partly covered with hydrophobic material, *Langmuir* (to be published), doi:10.1021/acs.langmuir.5b04703.
- [46] K. Yasui, A new formulation of bubble dynamics for sonoluminescence, Ph.D. thesis, Waseda University, 1996.
- [47] K. Yasui, Variation of liquid temperature at bubble wall near the sonoluminescence threshold, *J. Phys. Soc. Jpn.* **65**, 2830 (1996).
- [48] K. Yasui, Chemical reactions in a sonoluminescing bubble, *J. Phys. Soc. Jpn.* **66**, 2911 (1997).
- [49] D. L. Wise and G. Houghton, The diffusion coefficients of ten slightly soluble gases in water at 10–60 °C, *Chem. Eng. Sci.* **21**, 999 (1966).
- [50] K. Yasui, Effect of liquid temperature on sonoluminescence, *Phys. Rev. E* **64**, 016310 (2001).
- [51] P. W. Atkins, *Physical Chemistry*, 6th ed. (Oxford University Press, Oxford, 1998).
- [52] B. D. Storey and A. J. Szeri, Mixture segregation within sonoluminescence bubbles, *J. Fluid Mech.* **396**, 203 (1999).
- [53] R. C. Tolman, The effect of droplet size on surface tension, *J. Chem. Phys.* **17**, 333 (1949).
- [54] O. Wilhelmson, D. Bedeaux, and D. Reguera, Communication: Tolman length and rigidity constants of water and their role in nucleation, *J. Chem. Phys.* **142**, 171103 (2015).
- [55] M. N. Joswiak, N. Duff, M. F. Doherty, and B. Peters, Size-dependent surface free energy and Tolman-corrected droplet nucleation of TIP4P/2005 water, *J. Phys. Chem. Lett.* **4**, 4267 (2013).
- [56] M. E. M. Azouzi, C. Ramboz, J. F. Lenain, and F. Caupin, A coherent picture of water at extreme negative pressure, *Nat. Phys.* **9**, 38 (2013).
- [57] *CRC Handbook of Chemistry and Physics*, edited by D. R. Leid (CRC Press, Boca Raton, FL, 1994).
- [58] Y. An, Mechanism of single-bubble sonoluminescence, *Phys. Rev. E* **74**, 026304 (2006).
- [59] Y. S. Touloukian and T. Makita, *Specific Heat, Nonmetallic Liquids and Gases*, Thermophysical Properties of Matter, Vol. 6 (IFI/Plenum, New York, 1970).

- [60] K. Yasui, Effects of thermal conduction on bubble dynamics near the sonoluminescence threshold, *J. Acoust. Soc. Am.* **98**, 2772 (1995).
- [61] K. Yasui, Effect of surfactants on single-bubble sonoluminescence, *Phys. Rev. E* **58**, 4560 (1998).
- [62] Y. S. Touloukian, P. E. Liley, and S. C. Saxena, *Thermal Conductivity, Nonmetallic Liquids and Gases*, Thermophysical Properties of Matter, Vol. 3 (IFI/Plenum, New York, 1970).
- [63] F. Sharipov and V. Seleznev, Data on internal rarefied gas flows, *J. Phys. Chem. Ref. Data* **27**, 657 (1998).
- [64] S. Hilgenfeldt, D. Lohse, and M. P. Brenner, Phase diagrams for sonoluminescing bubbles, *Phys. Fluids* **8**, 2808 (1996).
- [65] K. Yasui, Influence of ultrasonic frequency on multibubble sonoluminescence, *J. Acoust. Soc. Am.* **112**, 1405 (2002).
- [66] K. Yasui, T. Tuziuti, J. Lee, T. Kozuka, A. Towata, and Y. Iida, Numerical simulations of acoustic cavitation noise with the temporal fluctuation in the number of bubbles, *Ultrason. Sonochem.* **17**, 460 (2010).
- [67] R. Hickling, Transient, High-Pressure Solidification Associated with Cavitation in Water, *Phys. Rev. Lett.* **73**, 2853 (1994).
- [68] D. L. Baulch, D. D. Drysdale, and D. G. Horne, *Evaluated Kinetic Data for High Temperature Reactions* (Butterworths, London, 1973), Vol. 2.
- [69] R. Mavrodineanu and H. Boiteux, *Flame Spectroscopy* (Wiley, New York, 1965), pp. 509–510.
- [70] K. Yasui, Unsolved problems in acoustic cavitation, in *Handbook of Ultrasonics and Sonochemistry*, edited by M. Ashokkumar (Springer, Singapore, 2016), pp. 259–292.
- [71] R. Battino, T. R. Rettich, and T. Tominaga, The solubility of nitrogen and air in liquids, *J. Phys. Chem. Ref. Data* **13**, 563 (1984).
- [72] R. Battino, T. R. Rettich, and T. Tominaga, The solubility of oxygen and ozone in liquids, *J. Phys. Chem. Ref. Data* **12**, 163 (1983).
- [73] T. R. Rettich, R. Battino, and E. Wilhelm, Solubility of gases in liquids. 18. High-precision determination of Henry fugacities for argon in liquid water at 2 to 40 °C, *J. Solution Chem.* **21**, 987 (1992).